

Article

Robust Backstepping Control with Active Damping Strategy for Separating-Metering Electro-Hydraulic System

Suhong Lin ¹, Gaocheng An ^{1,*}, Jiahai Huang ² and Yuhang Guo ³

¹ Coordinative Creation Center of Taiyuan Heavy Machinery Equipment, Taiyuan University of Science and Technology, Taiyuan 030024, China; suhong2011@foxmail.com

² Key Lab of Advanced Transducers and Intelligent Control System, Ministry of Education and Shanxi Province, Taiyuan University of Technology, Taiyuan 030024, China; huangjiahai@tyut.edu.cn

³ Department of Mechanical Engineering, Taiyuan Institute of Technology, Taiyuan 030008, China; guoyh@tit.edu.cn

* Correspondence: zyagc@tyust.edu.cn or zyagc@163.com; Tel.: +86-186-3682-5932

Received: 21 November 2019; Accepted: 25 December 2019; Published: 30 December 2019



Featured Application: The active damping strategy is proposed to suppress the oscillation in the separating-metering electro-hydraulic system. This work is suitable for the separating-metering system with low back pressure applications.

Abstract: Electro-hydraulic servo systems are widely used in industrial applications. The load greatly affects the dynamic response of the separating-metering electro-hydraulic system. The current researches mainly aim at the system tracking performance for the hydraulic servo system, but the researches on the damping characteristics are relatively less. For energy-saving reasons, the metering-out chamber is often maintained near a lower pressure. The system will oscillate when the load drastically changes. The active damping strategy is proposed in this work in order to increase the damping and suppress the oscillation in separating-metering electro-hydraulic system. The effectiveness of the active damping strategy is proven by mathematical derivation. Furthermore, the nonlinear mathematical model of the separating-metering electro-hydraulic system is built, and a robust backstepping controller that combines the tracking differentiator and nonlinear disturbance observer is designed. The experimental results indicate that the system oscillation is suppressed and the proposed controller has good tracking accuracy.

Keywords: electro-hydraulic servo system; separating-metering system; backstepping control; active damping control

1. Introduction

Heavy-duty machinery has many features, such as big load inertia, huge flow rate, and a vast amount of energy transmission; hence, hydraulic servo systems are widely used in those industrial applications. The separating-metering electro-hydraulic system (SMEHS) dismissed the mechanical linkage between the metering-in orifice and the metering-out orifice when compared with the traditional spool valve-controlled system, so the SMEHS has more freedom of degrees and it has more control flexibility [1–5]. However, the pressure of the cylinder metering-out chamber was often designed to be small to save energy. When the load force drastically changes, the SMEHS is easy to overshoot and oscillation, which means that the SMEHS does not have enough damping.

Some control schemes were developed by researchers to increase system damping [6–8]. Generally, these schemes fall into two categories. The first category is the “passive” damping scheme. These

schemes typically add accumulators or orifices to the hydraulic circuits [9] or they use the properties of the leakage and viscous friction to improve the system damping ratio. Although this technique is simple to use and easy to adjust, it causes energy loss and decreases the efficiency of the servo system under steady-state conditions. Besides, the passive damping scheme achieves limited damping effects; at the same time, it increases the nonlinearity of the servo system and then increases the difficulty when designing the controller. M Axin and P Krus analyzed the damping characters and presented a method to dimension the outlet orifice area in pressure compensated closed center mobile systems [10]. That method was a kind of passive damping method that transferred the kinetic energy into the thermal energy by the outlet orifice.

The second category is the “active” damping scheme. The term “active” means that these system parameters are monitored, and signals are generated to control the hydraulic actuators in such a way that the oscillations are cancelled out [11,12]. This method applied external energy into the system. Alexander A, Vacca A, and Cristofori D designed an active damping control law to suppress the vibration of the wheel loader [13]. A gain scheduler that was based on the real-time operating condition determined the parameters. R. Bell and A. De Pennington discussed the active compensation methods while using acceleration and pressure transducer signals in the electro-hydraulic servo system [14].

In this paper, the damping characteristics of the SMEHS are studied. The main contributions are: The novel active damping strategy for separating-metering electro-hydraulic system is proposed to increase the system damping, in which the robust backstepping controller with tracking differentiator and nonlinear disturbance observer is designed to increase the damping and suppress the oscillation.

The rest of this paper is organized, as follows. In Section 2, the active damping strategy is proposed and the effectiveness of the active damping strategy is theoretically proved. In Section 3, the mathematical model of SMEHS is developed. In Section 4, the robust backstepping controller with tracking differentiator and nonlinear disturbance observer is designed. In Section 5, the experiment and discussion are conducted. The last section presents the conclusions. Besides, there are many abbreviations in this paper. For ease of understanding, all the abbreviations and their definitions are listed in Nomenclature.

2. Problem Statement and Active Damping Strategy Analysis

For energy saving reasons, the pressure of the cylinder metering-out chamber was often designed at a lower level in the SMEHS. The system is easy to overshoot and oscillation when the load force drastically changes.

The active damping strategy (ADS) is proposed in order to improve the system damping and suppress the oscillation in the SMEHS (Figure 1). The active damping strategy establishes the correlation between the pressure of the metering-out chamber and the acceleration of the load. In the following, the damping ratio of the SMEHS is mathematically derived to prove the effectiveness of ADS.

Damping is the effect that tends to reduce the amplitude of vibrations [15], which means that the damping force always has the opposite direction with velocity. The pressure force at the metering-out chamber can be regarded as a damping force. As shown in Figure 2, when the rod is extending, the direction of the metering-out pressure force $F_{p_2A_2}$ is opposite to the rod moving direction, and there is a tendency to hinder the movement of the piston, so that the metering-out pressure force can be considered as a kind of damping for the system. The viscous damping force $F_{b\dot{x}}$ is also opposite to the speed direction and it is also the damping force of the system. Similarly, when the piston is retracted, as in Figure 3, the direction of the metering-out pressure force is opposite to the rod moving direction, so the metering-out pressure force $F_{p_1A_1}$ is a damping force of the system.

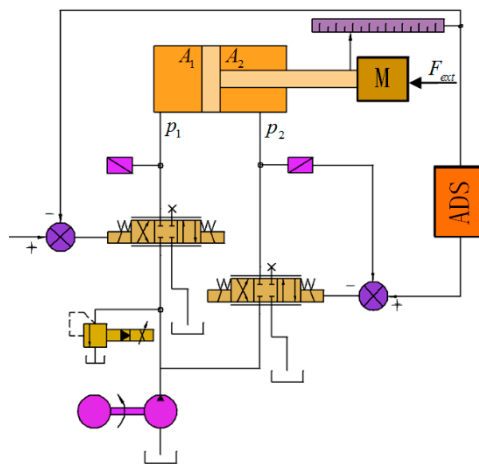


Figure 1. Separating-metering system with active damping strategy (ADS).

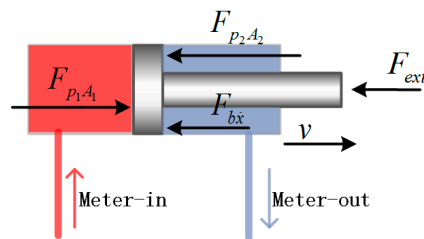


Figure 2. Rod is extending.

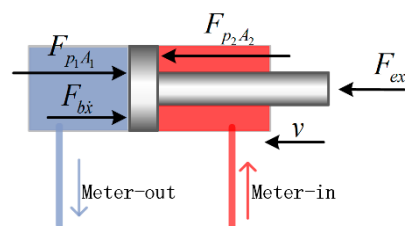


Figure 3. Rod is retracting.

Theoretical analysis is carried out to illustrate the characteristics of the ADS. Several assumptions are made, as follows:

1. The viscous damping coefficient and the leakages of the cylinder are ignored.
2. The friction force of piston in the cylinder is negligible.
3. The rod is extending.

The fluid flow through the servo valve orifice is given by the following equations:

$$q_1 = K_{v1}x_{v1} \sqrt{\Delta P_1} \tag{1}$$

$$q_2 = K_{v2}x_{v2} \sqrt{\Delta P_2} \tag{2}$$

where q_1 and q_2 are the flows through the valve, K_{v1} and K_{v2} are the valve coefficient of valve orifice, and ΔP_1 and ΔP_2 are pressure drops across the orifice, which are defined as:

$$\Delta P_i = \begin{cases} p_s - p_i, & x_{vi} \geq 0 \\ p_i - p_o, & x_{vi} < 0 \end{cases}, i = 1, 2 \tag{3}$$

where p_s is supply pressure and p_o is system tank pressure.

Equations (1) and (2) are needed to be linearized for the mathematical deduction. The following equations can be given while using Taylor’ series expansion.

$$q_1 = K_{v1}(K_{q1}x_{v1} - K_{c1}\Delta P_1) \tag{4}$$

$$q_2 = K_{v2}(K_{q2}x_{v2} - K_{c2}\Delta P_2) \tag{5}$$

where K_{q1} and K_{q2} are the flow coefficient and K_{c1} and K_{c2} are the flow-pressure coefficient. The pressure of cylinder chambers can be obtained by the fluid flow balance equations:

$$\dot{p}_1 = (q_1 - A_1\dot{x}_L) \frac{\beta_e}{V_{L1}} \tag{6}$$

where β_e is the effective bulk modulus of oil, p_1 is the pressure in piston chamber, V_{L1} is the volume of cylinder chambers, A_1 is the area of cylinder piston, and q_1 is the flow rate of cylinder. The force balance equation following Newton’s second law:

$$\ddot{x}_L = \frac{1}{m}(p_1A_1 - p_2A_2 - b\dot{x}_L - f_L) \tag{7}$$

where m is the total mass of the piston, f_L is the load force, and b is viscous damping coefficient. According to Equations (1), (3), (4), (6) and (7), the transfer function of SMEHS is derived as follows:

$$x_L = \frac{\frac{K_{q1}}{A_1}x_{v1} - \frac{1}{A_1^2}(K_{c1} + \frac{V_{L1}}{\beta_e}s)(A_2p_2 + f_L)}{s \cdot (\frac{s^2}{\omega_h^2} + \frac{2\zeta_h s}{\omega_h} + 1)} \tag{8}$$

where the natural frequency is given in Equation (9) and damping ratio is given in Equation (10).

$$\omega_h = A_1 \sqrt{\frac{\beta_e}{V_{L1}m}} \tag{9}$$

$$\zeta_h = \frac{K_c}{2A_1} \sqrt{\frac{\beta_e m}{V_{L1}}} \tag{10}$$

Therefore, the system block diagram is presented in Figure 4.

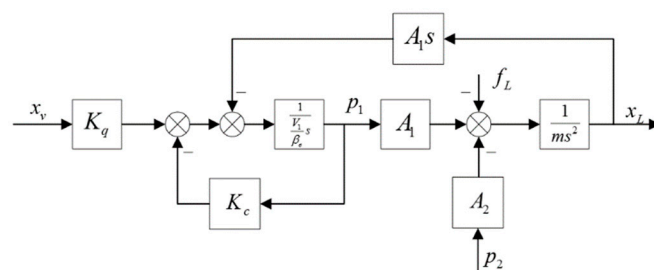


Figure 4. Block diagram of the separating-metering system.

It can be seen from Figure 4 that the spool displacement x_{v1} and the meter-out pressure p_2 affect the piston displacement x_L . In other words, this separating-metering system has two degrees of freedom. The ADS establish the correlation between p_2 and x_L , which is,

$$H_{af} = K_a s^2 \tag{11}$$

Figure 5 illustrates the block diagram of the separating-metering system with ADS.

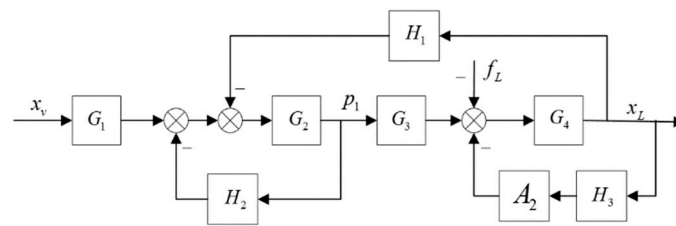


Figure 5. The system block diagram with the active damping strategy.

Substituting Equation (11) to Equation (8), the transfer function is presented:

$$x_L = \frac{\frac{K_a}{A_1}x_v - f_L \frac{1}{A_1^2} \left(\frac{V_{L1}}{\beta_e} s + K_c \right)}{s \left(\frac{s^2}{\omega_{h3}^2} + \frac{2\zeta_{h3}}{\omega_{h3}} s + 1 \right)} \tag{12}$$

where the damping ratio ζ_{h3} and natural frequency ω_{h3} are given by

$$\omega_{h3} = \sqrt{\frac{A_1^2 \beta_e}{V_{L1}(m + K_a)}} \tag{13}$$

$$\zeta_{h3} = \frac{K_c}{2A_1} \sqrt{\frac{\beta_e m}{V_{L1}}} + \frac{K_c}{2A_1} \sqrt{\frac{\beta_e K_a}{V_{L1}}} \tag{14}$$

Divided by Equation (9), Equation (13) is represented as follows.

$$\frac{\omega_{h3}}{\omega_h} = \sqrt{\frac{m}{m + K_a}} \tag{15}$$

Divided by Equation (10), Equation (14) is represented as follows.

$$\frac{\zeta_{h3}}{\zeta_h} = \sqrt{\frac{m + K_a}{m}} \tag{16}$$

Comparing Equations (10) and (14), it is clear that the ADS can improve the damping ratio in the system if $K_a > 0$. It is more apparent from (16) that the larger the value of K_a , the higher the damping ratio the system will have. However, comparing Equations (9) and (13), the eigenfrequency may become decreasing and the larger the value of K_a , the higher eigenfrequency the system will decrease.

3. Modeling of SMEHS

In Figure 1, the SMEHS consists of a hydraulic cylinder, a servo valve 1 at the metering-in side of the hydraulic cylinder, a servo valve 2 at the metering-out side, a hydraulic pump, and a relief valve. The two valves are used to control the cylinder. The two signals control the two independent valve spools, so the SMEHS has two degrees of freedom and it provides more flexibility and controllability. The relief valve is used to maintain a constant pressure of the system. The dynamics of the servo valve can be described by a second-order system, which yields the following equations, since the response frequency of the servo valve is much higher than that of the entire hydraulic system.

$$K_{s1} \omega_{v1}^2 u_1 = \ddot{x}_{v1} + 2\xi_{v1} \dot{x}_{v1} + \omega_{v1}^2 x_{v1} \tag{17}$$

$$K_{s2} \omega_{v2}^2 u_2 = \ddot{x}_{v2} + 2\xi_{v2} \dot{x}_{v2} + \omega_{v2}^2 x_{v2} \tag{18}$$

where x_{v1} and x_{v2} are the displacement of the servo valve spool, K_{s1} and K_{s2} are the servo valve gain, ω_{v1} and ω_{v2} are the natural frequency, ξ_{v1} and ξ_{v2} are damping ratio, and u_1 and u_2 are the input signal to servo valve.

The pressure dynamics can be obtained, as follows:

$$\dot{p}_1 = (q_1 - A_1\dot{x}_L) \frac{\beta_e}{V_{L01} + A_1x_L} + \Delta_1 \tag{19}$$

$$\dot{p}_2 = (q_2 + A_2\dot{x}_L) \frac{\beta_e}{V_{L02} - A_2x_L} + \Delta_2 \tag{20}$$

where β_e is the effective bulk modulus of oil, p_1 is the pressure in piston chamber, p_2 is the pressure in rod chamber, V_{L01} and V_{L02} are the initial volume of cylinder chambers, separately, including the chamber volume of connected pipeline, A_1 is the area of cylinder piston, A_2 is the effective actuating area of rod end in cylinder, x_L is the displacement of cylinder rod, Δ_1 and Δ_2 are uncertain terms due to parameter perturbation, modeling errors, and other disturbance.

While ignoring the mass of oil, we obtain the force balance equation following Newton’s second law:

$$\ddot{x}_L = \frac{1}{m}(p_1A_1 - p_2A_2 - b\dot{x}_L - f_L) + \Delta_3 \tag{21}$$

where m is the total mass of the piston, f_L is the load force, b is viscous damping coefficient, Δ_3 is the uncertain item, consisting of the external disturbance and unmodeled uncertainties.

3.1. Position Servo System of SMEHS

In Figure 1, servo valve 1 is used to control the displacement of the piston rod to track the given displacement signal x_d . Choosing u_i as the system input, and choosing x_L as the system output, the system state variable is presented, as follows.

$$x_i^T = [x_{i1} \quad x_{i2} \quad x_{i3} \quad x_{i4} \quad x_{i5}]^T = [x_L \quad \dot{x}_L \quad p_1 \quad x_{v1} \quad \dot{x}_{v1}]^T \tag{22}$$

Assuming that $\delta_{i2} = \frac{-p_2A_2}{m}$, $c_1 = \frac{A_1}{m}$, $c_2 = -b/m$, $c_3 = \frac{\beta_e}{V_{L1}} K_{v1} \sqrt{\Delta P_1}$, $c_4 = -\frac{\beta_e}{V_{L1}} A_1$, $c_5 = K_{s1}\omega_{v1}^2$, $c_6 = -\omega_{v1}^2$, $c_7 = -2\omega_{v1}\xi_{v1}$, $V_{L1} = V_{L01} + A_1x_L$, the state-space function of the metering-in side can be illustrated, as follows.

$$\begin{cases} \dot{x}_{i1} = x_{i2} \\ \dot{x}_{i2} = c_1x_{i3} + c_2x_{i2} + \delta_{i2} + \theta_{i2} \\ \dot{x}_{i3} = c_3x_{i4} + c_4x_{i2} + \theta_{i3} \\ \dot{x}_{i4} = x_{i5} \\ \dot{x}_{i5} = c_5u_i + c_6x_{i4} + c_7x_{i5} \end{cases} \tag{23}$$

where θ_{i2} and θ_{i3} are the disturbance combining of uncertainties, unmodeled items, and external disturbances in the model. In Section 4.1, a disturbance observer is designed to compensate for the disturbance in order to achieve perfect dynamic performance.

3.2. Pressure Servo System of SMEHS

In Figure 1, servo valve 2 is used to control the pressure of the metering-out chamber to track the given signal p_d . Choosing u_o as the system input, and choosing p_2 as the system output, the system state variable is presented, as following.

$$x_o^T = [x_{o1} \quad x_{o2} \quad x_{o3}]^T = [p_2 \quad x_{v2} \quad \dot{x}_{v2}]^T \tag{24}$$

Assuming that $\delta_{o1} = \frac{\beta_e}{V_{L2}} A_2 \dot{x}_L$, $d_1 = \frac{\beta_e}{V_{L2}} K_{v2} \sqrt{\Delta P_2}$, $d_2 = K_{s2} \omega_{v2}^2$, $d_3 = -2\xi_{v2} \omega_{v2}$, $V_{L2} = V_{L02} + A_1 x_L$, $d_4 = -\omega_{v2}^2$, the dynamic state function of the metering-in side can be illustrated, as follows.

$$\begin{cases} \dot{x}_{o1} = d_1 x_{o2} + \delta_{o1} + \theta_{o1} \\ \dot{x}_{o2} = x_{o3} \\ \dot{x}_{o3} = d_2 u_o + d_3 x_{o3} + d_4 x_{o2} \end{cases} \quad (25)$$

Similarly, θ_{o1} is the combining of disturbances due to unmodeled and external disturbances items in the model. In Section 4.1, a disturbance observer is designed to compensate for the disturbance.

4. Controller Design

There are many control algorithms for hydraulic servo systems [16–19]. Wang C, Quan L, and Zhang S developed the active disturbance rejection control (ADRC) algorithm [20], which avoided the high stiffness control and mismatched uncertainties input, and the hydraulic servo system obtained an excellent tracking performance. Choux M, Karimi H, and Hovland G presented a backstepping technique based adaptive controller to make sure that the tracking error converges to zero asymptotically to overcome the uncertainties in the system according to the Barbalat lemma [21]. M.Hast, K.J.Astrom, et al. proposed the Convex-Concave optimization method for the PID (proportional–integral–derivative) controller [22,23]. Karimi and Kammer proposed a robust controller that is based on convex optimization [24]. Niksefat N and Sepehri N designed a robust force controller that is based on nonlinear quantitative feedback theory to overcome uncertainties in the industrial hydraulic system [25]. The designed controller satisfied the tracking performance, and it was low-order, which was easily implemented in the industry. Truong DQ and Ahn KK used a grey prediction based fuzzy PID controller for eliminating the disturbance and improving the control quantity of the system [26]. The system had excellent dynamic characteristics, but it was hard to tune the controller parameters.

Backstepping control is useful for dealing with uncertainty in nonlinear systems. In recent years, many researchers have conducted several studies on this algorithm. Na Jing proposed a new control design method for high-order servo systems with hydraulic actuator dynamics [27]. The results showed that the combined controller improved dynamic performance. Wang Y and Wu H designed a backstepping controller, in which unknown uncertainties are approximated while using neural networks [28]. However, the complexity of the backstepping controller dramatically increases as the order of the system increases, which is called “computational explosion”, due to the classic backstepping method requiring repeated derivation of the signal. A dynamic surface control method was utilized in order to solve this problem [29–31]. It was shown that this method helped to deal with the “computational explosion” problem.

Based on the above research, the robust backstepping controller combining with a tracking differentiator (TD) and a nonlinear disturbance observer (NDO) is proposed in this section, which is called BSTDNDO for short. The BSTDNDO is used to control the cylinder to track the reference signals. TD is applied in the controller to avoid “computational explosion”. The NDO is used to compensate for the uncertainties and disturbances. Figure 6 shows the structure of the proposed controller.

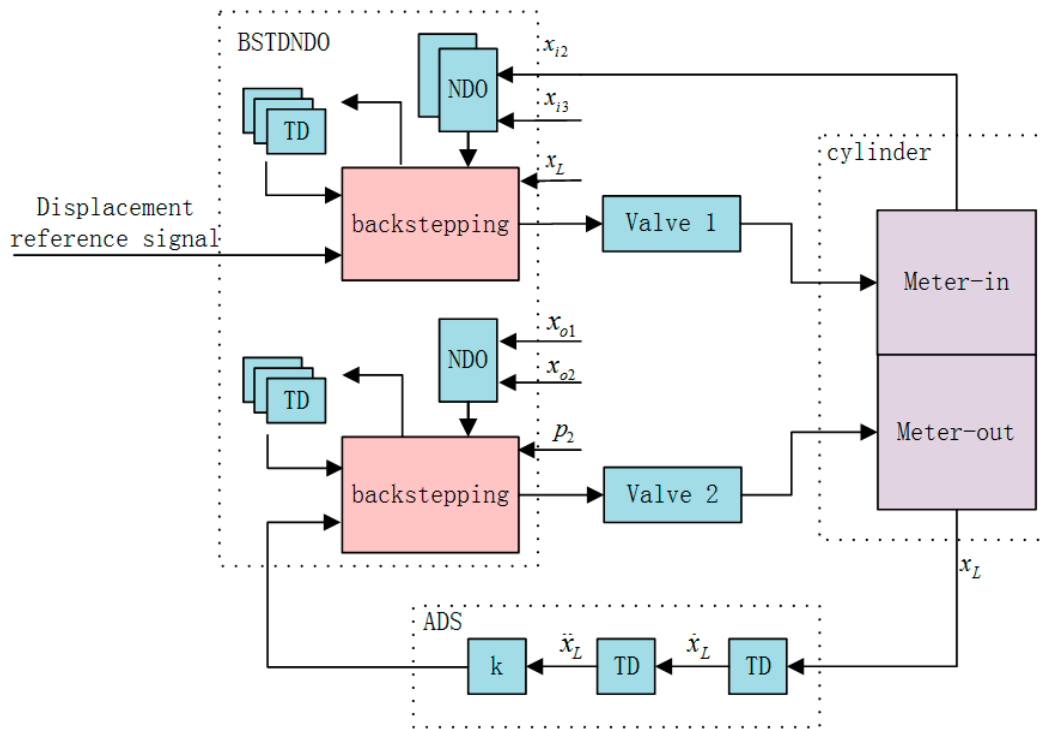


Figure 6. Block diagram of the proposed control strategy.

4.1. Nonlinear Disturbance Observer

The uncertainties and disturbances in the system must be adequately compensated in order to achieve perfect tracking performance. A nonlinear disturbance observer is utilized to deal with this problem. The nonlinear disturbance observer is designed, as follows [32].

$$\begin{cases} \hat{\theta}_{i2} = \sigma_{i2} + \eta_{i2}x_{i2} \\ \dot{\sigma}_{i2} = -\eta_{i2}\sigma_{i2} - \eta_{i2}(c_1x_{i3} + c_2x_{i2} + \delta_{i2} + \eta_{i2}x_{i2}) \end{cases} \quad (26)$$

$$\begin{cases} \hat{\theta}_{i3} = \sigma_{i3} + \eta_{i3}x_{i3} \\ \dot{\sigma}_{i3} = -\eta_{i3}\sigma_{i3} - \eta_{i3}(c_3x_{i4} + c_4x_{i2} + \eta_{i3}x_{i3}) \end{cases} \quad (27)$$

$$\begin{cases} \hat{\theta}_{o1} = \sigma_{o1} + \eta_{o1}x_{o1} \\ \dot{\sigma}_{o1} = -\eta_{o1}\sigma_{o1} - \eta_{o1}(d_1x_{o2} + \delta_{o1} + \eta_{o1}x_{o1}) \end{cases} \quad (28)$$

where η_{i2} , η_{i3} , and η_{o1} are the gains of the observer, which are related to the convergence speed of the NDO. σ_{i2} , σ_{i3} , and σ_{o1} are the internal variables.

4.2. Tracking Differentiator

In engineering applications, differential methods usually obtain the derivative of the signal. However, when the noise mixed in the signal, this method will amplify the noise. The tracking differentiator is proposed to solve this problem. The tracking differentiator is designed, as follows [33].

$$\begin{cases} \dot{x}_1 = x_2 \\ \dot{x}_2 = -r^2 \text{sign}(x_1 - x_{in}) \cdot (x_1 - x_{in})^\alpha - rx_2 \end{cases} \quad (29)$$

where x_{in} is the input of TD, x_1 is the tracking output of x_{in} , x_2 is the derivative of the input x_{in} , r is the gain of TD, and it is positive, which determines the tracking speed of TD. α is limited by $0 < \alpha < 1$, which determines the approaching speed of TD.

4.3. Backstepping Controller Design

The the metering-in valve controls rod displacement x_{i1} to track the reference displacement signal x_d . The metering-out valve to track the reference signal p_d controls the metering-out chamber pressure p_2 . For the metering-in side servo system, BSTDNDO is designed in five steps. A similar design procedure is utilized for the metering-out servo system to build a pressure regulator, which is omitted. Throughout this paper, $\hat{\bullet}$ is used to denote the estimate of \bullet , $\tilde{\bullet}$ is used to denote the estimation error of \bullet . According to (23),

Step 1: The displacement tracking error e_1 is defined, as follows.

$$e_1 = x_{i1} - x_d \tag{30}$$

where x_d is the given reference signal for the tracking system. Define $e_2 = x_{i2} - \alpha_1$, where α_1 is the first virtual control variable, it is presented, as follows.

$$\alpha_1 = -k_1 e_1 + \dot{x}_d \tag{31}$$

where k_1 is the controller gain, $k_1 > 0$. The derivative of Equation (30) is

$$\dot{e}_1 = \dot{x}_{i1} - \dot{x}_d = x_{i2} - \dot{x}_d = e_2 + \alpha_1 - \dot{x}_d \tag{32}$$

If α_1 is treated as the virtual control input, then the subsystem (32) can converge to zero or as small as possible. Selecting the positive semi-definite Lyapunov function $V_1 = \frac{1}{2}e_1^2$ obtains its time derivative:

$$\dot{V}_1 = e_1 \dot{e}_1 = e_1(e_2 + \alpha_1 - \dot{x}_d) = -k_1 e_1^2 + e_1 e_2 \tag{33}$$

It is easy to know that, if e_2 converges to zero and $k_1 > 0$, then e_1 can converge to zero in finite time by choosing the proper controller gain k_1 .

Step 2: In this step, we need to design the controller to make sure that e_2 can converge to zero. Define the error $e_3 = x_{i3} - \alpha_2$, where α_2 is the second virtual control variable and it is defined, as follows.

$$\alpha_2 = \frac{1}{c_1}(-k_2 e_2 - c_2(e_2 + \alpha_1) - \hat{\theta}_2 - \delta_2 - e_1 + \hat{\alpha}_1) \tag{34}$$

In Equation (34), k_2 is the controller gain, $k_2 > 0$. $\hat{\alpha}_1$ is obtained by TD. $\hat{\theta}_2$ is obtained by NDO. The derivative of e_2 is:

$$\dot{e}_2 = \dot{x}_{i2} - \dot{\alpha}_1 = c_1 x_3 + c_2 x_{i2} + \theta_2 + \delta_2 - \dot{\alpha}_1 \tag{35}$$

The following equation is obtained when the Lyapunov function signal is chosen to be $V_2 = V_1 + \frac{1}{2}e_2^2$.

$$\dot{V}_2 = -k_1 e_1^2 - k_2 e_2^2 + c_1 e_2 e_3 + e_2 \tilde{\theta}_2 - e_2 \tilde{\alpha}_1 \tag{36}$$

In Equation (36), if e_3 converge to zero, then e_2 can converge to zero in finite time by choosing the proper controller gain k_2 .

Step 3: In this step, we need to design the controller to make sure that e_3 can converge to zero. Define $e_4 = x_4 - \alpha_3$, where α_3 is the third virtual control variable, and it is defined, as follows.

$$\alpha_3 = \frac{1}{c_3}(-k_3 e_3 - c_4(e_2 + \alpha_1) - \hat{\theta}_3 + \hat{\alpha}_2 - c_1 e_2) \tag{37}$$

In Equation (37), $\hat{\alpha}_2$ is obtained by TD, $\hat{\theta}_3$ is obtained by NDO. k_3 is the controller gain, $k_3 > 0$. The derivative of e_3 is obtained, as follows.

$$\dot{e}_3 = \dot{x}_3 - \dot{\alpha}_2 = c_3 x_4 + c_4(e_2 + \alpha_1) + \theta_3 - \dot{\alpha}_2 \tag{38}$$

The following equation is obtained when the Lyapunov function signal is chosen to be $V_3 = V_2 + \frac{1}{2}e_3^2$.

$$\dot{V}_3 = -k_1e_1^2 - k_2e_2^2 - k_3e_3^2 + e_2\tilde{\theta}_2 + e_3\tilde{\theta}_3 - e_2\tilde{\alpha}_1 - e_3\tilde{\alpha}_2 + c_3e_3e_4 \tag{39}$$

It is easy to know that if e_4 converges to zero and $k_3 > 0$, then e_3 can converge to zero in finite time by choosing the proper controller gain k_3 .

Step 4: In this step, we need to design the controller to make sure that e_4 can converge to zero. Define $e_5 = x_5 - \alpha_4$, where α_4 is the virtual control variable.

$$\alpha_4 = -k_4e_4 + \hat{\alpha}_3 - c_3e_3 \tag{40}$$

where $\hat{\alpha}_3$ is the estimate of α_3 , it is obtained by TD, k_4 is the controller gain, $k_4 > 0$.

The derivative of e_4 is

$$\dot{e}_4 = e_5 + \alpha_4 - \dot{\alpha}_3 \tag{41}$$

When the Lyapunov function signal is chosen to be $V_4 = V_3 + \frac{1}{2}e_4^2$, the following equation is obtained.

$$\dot{V}_4 = -k_1e_1^2 - k_2e_2^2 - k_3e_3^2 - k_4e_4^2 + e_2\tilde{\Delta}_2 + e_3\tilde{\Delta}_3 - e_2\tilde{\alpha}_1 - e_3\tilde{\alpha}_2 - e_4\tilde{\alpha}_3 + e_4e_5 \tag{42}$$

In Equation (42), if e_5 converge to zero then e_4 can converge to zero in finite time by choosing the proper controller gain k_4 .

Step 5: In the last step, we consider the convergence of e_5 to make sure that e_5 can converge to zero. The derivative of e_5 is shown as

$$\dot{e}_5 = c_5u_1 + c_6x_4 + c_7x_5 - \dot{\alpha}_4 \tag{43}$$

The control law u_i can be deduced, as follows.

$$u_i = \frac{1}{c_5}[-k_5e_5 - c_6(e_4 + \alpha_3) - c_7(e_5 + \alpha_4) - e_4 + \hat{\alpha}_4] \tag{44}$$

where $\hat{\alpha}_4$ is obtained by TD and k_5 is the controller gain, $k_5 > 0$.

4.4. Stability Analysis of Nonlinear Disturbance Observer

Consider the following system in order to analysis the stability of NDO:

$$\dot{x}_i = g(\bar{x}_i) \cdot x_{i+1} + f(\bar{x}_i) + d_i \tag{45}$$

where d_i denotes the disturbance of the system, and \bar{x}_i denotes (x_1, x_2, \dots, x_i) . Generally, due to the disturbance is uncertain, we assume that $\dot{d}_i = 0$. The NDO for the system represented by the Equation (45) is presented, as follows.

$$\begin{cases} \dot{\hat{d}}_i = z_i + p_i(\bar{x}_i) \\ \dot{z}_i = -L_i \cdot z_i - L_i \cdot (p_i(\bar{x}_i) + g(\bar{x}_i) \cdot x_{i+1} + f(\bar{x}_i)) \end{cases} \tag{46}$$

where z_i is the internal variable and L_i is the gain for NDO. The estimating error of d_i is defined as

$$\tilde{d}_i = d_i - \hat{d}_i \tag{47}$$

The Lyapunov function is chosen in order to analysis the stability of NDO, as follows

$$V = \frac{1}{2}\tilde{d}_i^2 \tag{48}$$

Differentiating the Lyapunov function (48), Equation (49) is obtained.

$$\dot{V} = \tilde{d}_i \cdot \dot{\tilde{d}}_i = \tilde{d}_i \cdot (\dot{d}_i - \tilde{d}_i) = -L_i \tilde{d}_i^2 \tag{49}$$

By choosing positive L_i , the stability can be proofed, and the desired exponential convergence rate is related to the value of L_i .

4.5. Stability Analysis of BSTDNDO

The Lyapunov function is chosen to be: $V_i = V_4 + \frac{1}{2}e_5^2$ in order to evaluate the stability. This results in Equation (50).

$$\dot{V}_i = -k_1e_1^2 - k_2e_2^2 - k_3e_3^2 - k_4e_4^2 - k_5e_5^2 + e_2\tilde{\Delta}_2 + e_3\tilde{\Delta}_3 - e_2\tilde{\alpha}_1 - e_3\tilde{\alpha}_2 - e_4\tilde{\alpha}_3 - e_5\tilde{\alpha}_4 \tag{50}$$

The error of TD is also bounded because selecting proper parameters bound the tracking error of NDO. According (50), Equation (51) is obtained.

$$\dot{V}_i \leq -k(e_1^2 + e_2^2 + e_3^2 + e_4^2 + e_5^2) + |e_2|\tilde{\Delta}_2 + |e_3|\tilde{\Delta}_3 + |e_2|\tilde{\alpha}_1 + |e_3|\tilde{\alpha}_2 + |e_4|\tilde{\alpha}_3 + |e_5|\tilde{\alpha}_4 \tag{51}$$

Equation (51) can be rewritten, as follows.

$$\dot{V}_i \leq -2(k-1)V_i + \frac{1}{2}\varepsilon^2 \tag{52}$$

where $k = \min\{k_1, k_2, k_3, k_4, k_5\}$ and $\varepsilon = |\tilde{\Delta}_2| + |\tilde{\Delta}_3| + |\tilde{\alpha}_1| + |\tilde{\alpha}_2| + |\tilde{\alpha}_3| + |\tilde{\alpha}_4|$.

Solving the Inequality (52), the non-negative Lyapunov function V_i is bounded by

$$V_i \leq [V_i(0) - \frac{\varepsilon^2}{4(k-1)}]e^{-2(k-1)t} + \frac{\varepsilon^2}{4(k-1)} \tag{53}$$

By choosing any positive number φ and $k \geq 1 + \frac{\varepsilon^2}{4\varphi}$, if $V_i(0) \leq \varphi$, then $V_i(t) \leq \varphi$ will be guaranteed for all $t > 0$. Therefore, the controller stability is proven, and the tracking error can converge to a sufficient small neighbor of zero.

5. Experiment and Discussion

5.1. Experiment Platform

A test rig has been constructed in order to validate the proposed control strategy. Figure 7 briefly depicts the schematic of the hydraulic system of the test rig. It consists of a position tracking system and a loading system. The position tracking system consists of cylinder 5, servo valve3.1 and 3.2, pressure sensor4, relief valve2.1 and 2.2, and fixed displacement pump1.1 and 1.2. The cylinder 5 is controlled by two servo valves, respectively. The max system pressure is determined by the crack pressure of the relief valve. Pressure sensors are attached to both cylinder chambers. The cylinder is equipped with a displacement sensor. The loading system is used to maintain a constant load force that is applied to cylinder 5. The direction of the loading force can be controlled by directional valve 9, and the magnitude of the loading force can be regulated by relief valve 2.2. Table 1 provides the main specifications of the test rig. Figure 8 shows a photo of the test rig.

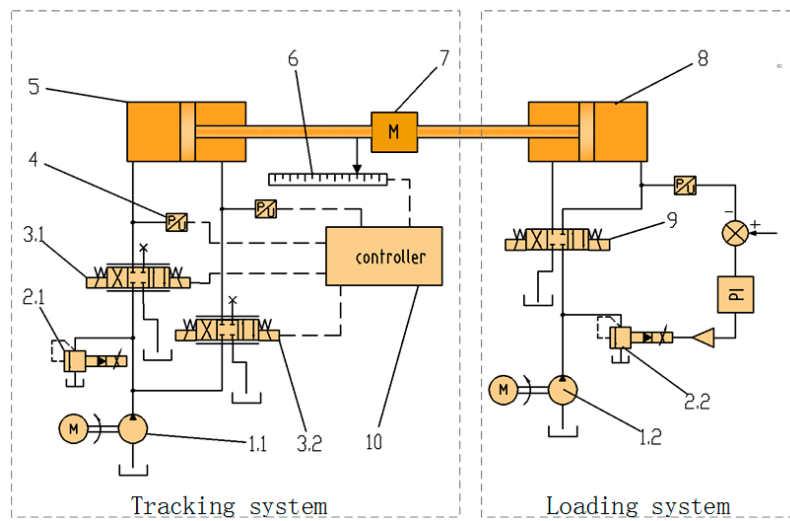


Figure 7. The schematic of the hydraulic system for the test rig; 1.1,1.2-fixed displacement pump; 2.1,2.1-relief valve; 3.1,3.2-servo valve; 4—pressure sensor; 5—testing cylinder; 6—displacement sensor; 7—mass block; 8—loading cylinder; 9—directional valve; and, 10—controller.

Table 1. Main Specifications of the Test Rig.

Item	Value	Unit
Pump displacement (1.1 and 1.2)	40	mL/r
Motor speed	1500	rpm
Servo valve rated flow (3.1)	63	L/min
Servo valve rated flow (3.2)	38	L/min
Piston diameter (5 and 8)	63	mm
Rod diameter (5 and 8)	36	mm
Weight of moving part	100	Kg
Stroke (5 and 8)	280	mm

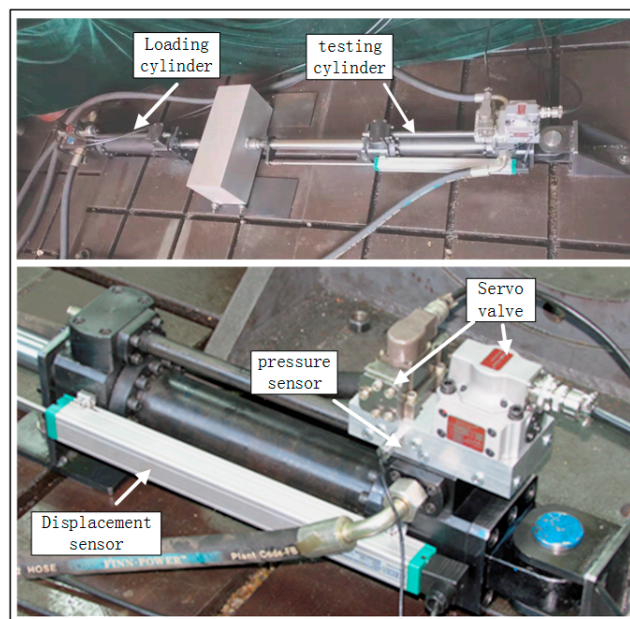


Figure 8. The photo of the test rig.

5.2. Displacement Tracking Experiments

Comparative experiments were carried out in order to test the tracking performance of BSTDNDO. Figure 9 shows the reference signal. The constant load force was adjusted to 50 kN and applied to the cylinder during the experiments. The metering-out valve kept the maximum orifice opening. The parameters of BSTDNDO were $k_1 = 55, k_2 = 35, k_3 = 230, r = 40, \alpha = 0.8, \eta_{i2} = 200, \eta_{i3} = 100,$ and $\eta_{o1} = 100$. The max tracking error of BSTDNDO was 2.35 mm, as shown in Figure 10. Subsequently, comparative experiments were carried out. Because the sliding mode control (SMC) algorithm was robust and practical in engineering [34–36], it was chosen for this comparison. A large number of parameter sets were tested to make sure that the SMC controller works with the highest performance. Figure 11 shows the tracking error while using the SMC algorithm. The BSTDNDO controller had higher tracking accuracy than the SMC controller because the uncertainties and disturbances were observed by NDO and compensated during the controller design procedure (Figures 12 and 13). The max displacement tracking error was 3.62 mm and the maximum tracking error was reduced by 35%.

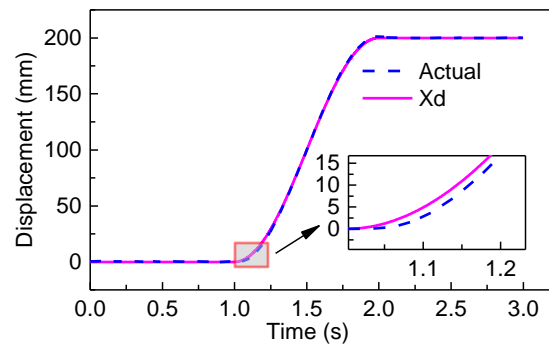


Figure 9. Displacement tracking using backstepping controller with tracking differentiator and nonlinear disturbance observer (BSTDNDO).

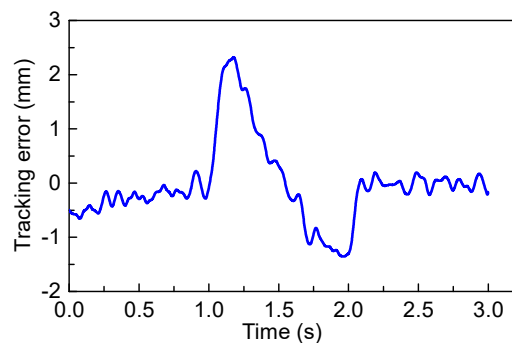


Figure 10. Tracking error using BSTDNDO.

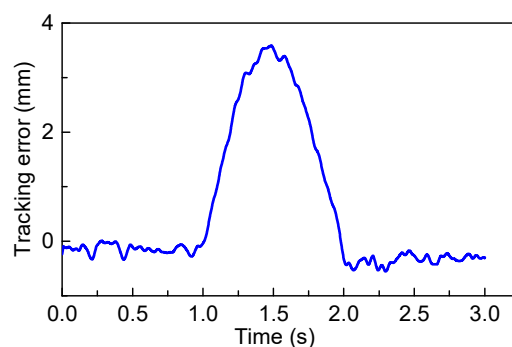


Figure 11. Tracking error using sliding mode control (SMC).

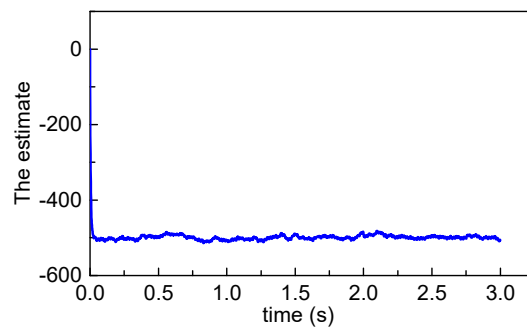


Figure 12. The estimate of θ_{i2} .

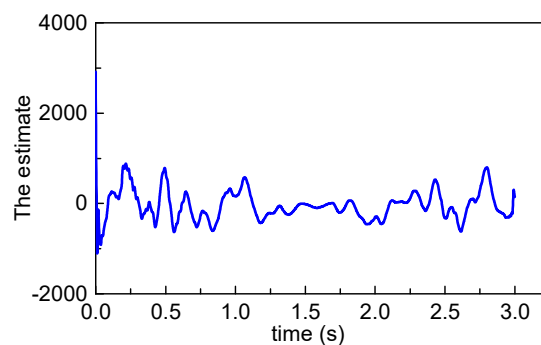


Figure 13. The estimate of θ_{i3} .

5.3. Active Damping Strategy Experiments

Another experiment was carried out in order to verify the effectiveness of ADS. In this experiment, a slope signal was chosen as the reference signal, as shown in Figure 14. The ADS was disabled during the experiments. The pressure of the metering-out chamber was regulated to 25 bar. The load force was adjusted to 50 kN. When $t = 1\text{ s}$, the load force suddenly decreased to zero. The oscillation occurred due to the low pressure at the metering-out chamber. Figure 15 shows the rod displacement. The system started to oscillate from $t = 1\text{ s}$ and became stable until $t = 1.22\text{ s}$, the oscillation occurred for 0.22 s. The maximum overshoot was 15.2 mm. Figure 16 shows the pressure of both the metering-in side and the metering-out side.

The comparative experiment was carried out and the ADS was enabled. The load force was adjusted to 50 kN. The load force suddenly decreased to zero when $t = 1\text{ s}$. The system started to oscillate from $t = 1\text{ s}$ and it became stable until $t = 1.13\text{ s}$. The oscillation occurred for 0.13 s. The maximum overshoot was 13.6 mm. Figure 17 shows the pressure of both the metering-in side and the metering-out side. The ADS played a vital role to raise the metering-out reference signal when the rod displacement began to oscillate. The oscillation time was reduced by 41% and the maximum overshoot was reduced by 10.5% when compared with the results of the experiments.

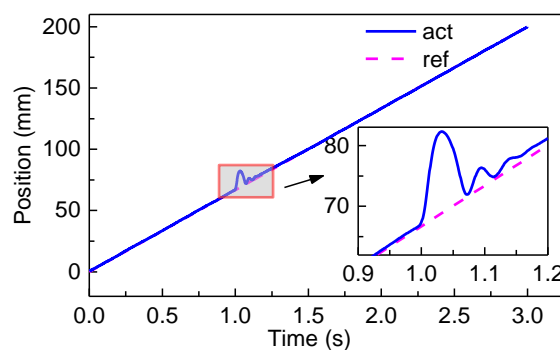


Figure 14. Position tracking under external force disturbance (without ADS).

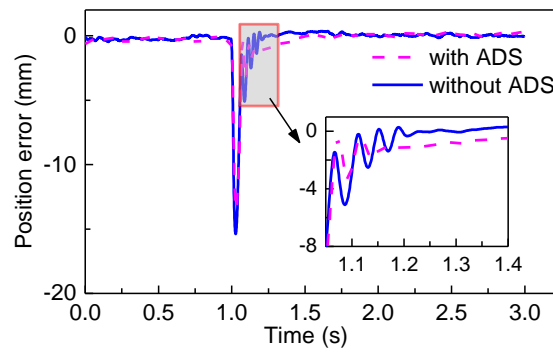


Figure 15. Position error (ADS restrained oscillation).

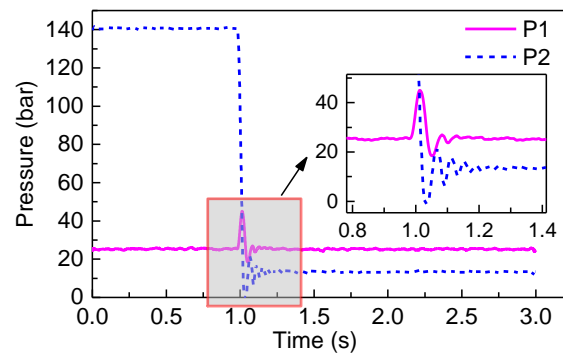


Figure 16. The pressure of cylinder chambers without ADS.

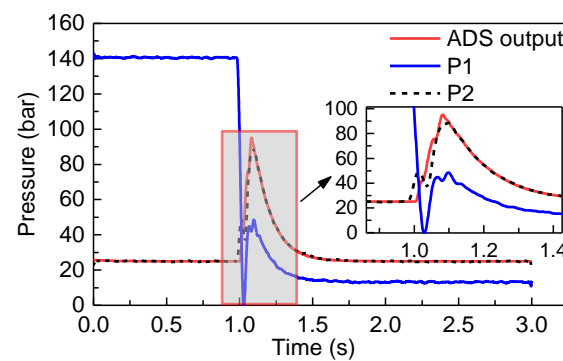


Figure 17. The pressure of cylinder chambers with ADS.

6. Conclusions

The metering-out chamber in SMEHS is often maintained near a lower pressure for energy-saving reasons. When the load drastically changes, the system is easy to oscillate. The damping characteristics of SMEHS are investigated and the novel active damping strategy is proposed in this work in order to suppress the oscillation.

A robust backstepping controller combining with tracking differentiator and nonlinear disturbance observer is designed for the separating-metering electro-hydraulic system with the active damping strategy. The experimental results indicate that, when compared with the SMC controller, the maximum tracking error is reduced by 35%. By using the active damping strategy, the duration of oscillation time is reduced by 41%. The maximum overshoot is reduced by 10.5%.

In summary, the proposed controller has excellent tracking performance, and the proposed active damping strategy effectively suppresses the oscillation. This work is suitable for the separating-metering system with low back pressure applications. However, the metering out chamber pressure will get increased, which means that the system has lower energy efficiency in order to increase loop damping.

Therefore, how to improve the energy efficiency of the active damping strategy in SMEHS is one of the issues to be addressed in the future.

Author Contributions: Data curation, S.L.; Funding acquisition, G.A.; Investigation, S.L. and Y.G.; Methodology, S.L. and J.H.; Project administration, G.A.; Software, S.L. and Y.G.; Supervision, J.H.; Validation, J.H.; Writing—original draft, S.L.; Writing—review & editing, J.H. All authors have read and agreed to the published version of the manuscript.

Funding: This work reported here is funded by the Coordinative Creation Center of Taiyuan Heavy Machinery Equipment of China (1331 Project).

Conflicts of Interest: The authors declare that there is no conflict of interests regarding the publication of this paper.

Nomenclature

A_1, A_2	area of piston
ADRC	active disturbance rejection control
ADS	active damping strategy
b	viscous damping coefficient
BSTDNDO	backstepping controller with TD and NDO
$c_1, c_2, c_3, c_4, c_5, c_6, c_7$	internal variable
d_1, d_2, d_3, d_4	internal variable
d_i	disturbance
e_1, e_2, e_3, e_4, e_5	tracking error
$F_{b\dot{x}}$	viscous damping force
f_L	load force
$F_{p_1A_1}$	force exerting on the piston of the cylinder in rod chamber
$F_{p_2A_2}$	force exerting on the piston of the cylinder in piston chamber
k	internal variable
k_1, k_2, k_3, k_4, k_5	gain of controller
K_a	pressure-acceleration coefficient
K_{c1}, K_{c2}	flow-pressure coefficient
K_{q1}, K_{q2}	flow coefficient
K_{s1}, K_{s2}	servo valve gain
K_{v1}, K_{v2}	valve coefficient of the orifice
L_i	gain of NDO
m	equivalent mass of piston and attached system
NDO	nonlinear disturbance observer
p_1	pressure of piston chamber
p_2	pressure of rod chamber
p_o	pressure of oil tank
p_s	supply pressure
PID	proportional–integral–derivative
q_1	flow rate of piston chamber
q_2	flow rate of rod chamber
r	gain of tracking differentiator
s	Laplace Operator
$sign(\bullet)$	signum function
SMC	sliding mode control
SMEHS	separating-metering electro-hydraulic system
TD	tracking differentiator
u_1, u_2, u_i, u_o	input signal
V_{L1}, V_{L2}	volume of hydraulic chamber
V_{L01}, V_{L02}	initial volume of chamber
$V, V_1, V_2, V_3, V_4, V_i$	Lyapunov function

x_d	desired displacement of the piston
x_{in}	input of tracking differentiator
\bar{x}_i	denotes (x_1, x_2, \dots, x_i)
x_L	piston displacement
x_{v1}, x_{v2}	displacement of spool
x_i, x_o	state variables
z_i	internal variable
$\hat{\bullet}$	denote the estimate value of \bullet
$\tilde{\bullet}$	denote the estimation error of \bullet
$\Delta P_1, \Delta P_2$	pressure drops across the orifice
$\Delta_1, \Delta_2, \Delta_3$	uncertain item
α	parameter of tracking differentiator
$\alpha_1, \alpha_2, \alpha_3, \alpha_4$	virtual parameters
$\theta_{i2}, \theta_{i3}, \theta_{o1}$	disturbance
ω_h, ω_{h3}	natural frequency
ζ_h, ζ_{h3}	damping ratio
β_e	bulk modulus
δ_{i2}	internal variable
$\eta_{i2}, \eta_{i3}, \eta_{o1}$	gain of observer
$\sigma_{i2}, \sigma_{i3}, \sigma_{o1}$	internal variable
ε	internal variable
x_d	desired displacement of the piston
x_{in}	input of tracking differentiator
\bar{x}_i	denotes (x_1, x_2, \dots, x_i)
x_L	piston displacement
x_{v1}, x_{v2}	displacement of spool
x_i, x_o	state variables
z_i	internal variable
$\hat{\bullet}$	denote the estimate value of \bullet
$\tilde{\bullet}$	denote the estimation error of \bullet
$\Delta P_1, \Delta P_2$	pressure drops across the orifice
$\Delta_1, \Delta_2, \Delta_3$	uncertain item
α	parameter of tracking differentiator
$\alpha_1, \alpha_2, \alpha_3, \alpha_4$	virtual parameters
$\theta_{i2}, \theta_{i3}, \theta_{o1}$	disturbance
ω_h, ω_{h3}	natural frequency
ζ_h, ζ_{h3}	damping ratio
β_e	bulk modulus
δ_{i2}	internal variable
$\eta_{i2}, \eta_{i3}, \eta_{o1}$	gain of observer
$\sigma_{i2}, \sigma_{i3}, \sigma_{o1}$	internal variable
ε	internal variable

References

1. Lyu, L.; Chen, Z.; Yao, B. Development of Pump and Valves Combined Hydraulic System for Both High Tracking Precision and High Energy Efficiency. *IEEE Trans. Ind. Electron.* **2019**, *66*, 7189–7198. [[CrossRef](#)]
2. Liu, K.; Gao, Y.; Tu, Z. Energy saving potential of load sensing system with hydro-mechanical pressure compensation and independent metering. *Int. J. Fluid Power* **2016**, *17*, 173–186. [[CrossRef](#)]
3. Liu, B.; Quan, L.; Ge, L. Research on the performance of hydraulic excavator with pump and valve combined separate meter in and meter out circuits. *Chin. J. Mech. Eng.* **2016**, *52*, 173–180.
4. Choi, K.; Seo, J.; Nam, Y.; Kim, K.U. Energy-saving in excavators with application of independent metering valve. *J. Mech. Sci. Technol.* **2015**, *29*, 387–395. [[CrossRef](#)]
5. Lu, L.; Yao, B. Energy-Saving Adaptive Robust Control of a Hydraulic Manipulator Using Five Cartridge Valves with an Accumulator. *IEEE Trans. Ind. Electron.* **2014**, *61*, 7046–7054. [[CrossRef](#)]

6. Williamson, C.; Lee, S.; Ivantysynova, M. Active Vibration Damping for an Off-Road Vehicle with Displacement Controlled Actuators. *Int. J. Fluid Power* **2009**, *10*, 5–16. [[CrossRef](#)]
7. Nevala, K.; Jarviluoma, M. An active vibration damping system of a driver's seat for off-road vehicles. In *Mechatronics and Machine Vision in Practice*; IEEE: Queensland, Australia, 1997; p. 38.
8. Brecher, C.; Schulz, A.; Week, M. Electrohydraulic Active Damping System. *Cirp Ann. Manuf. Technol.* **2005**, *54*, 389–392. [[CrossRef](#)]
9. Palmer, M.K.; Simkus, V.A.; Beaudin, C.P.; Vogt, B.A. Ride Control System. U.S. Patent US5733095A, 31 March 1998.
10. Axin, M.; Krus, P. Design Rules for High Damping in Mobile Hydraulic Systems. In Proceedings of the Scandinavian International Conference on Fluid Power—Sicfp, Linköping, Sweden, 3–5 June 2013.
11. Rahmfeld, R.; Ivantysynova, M. An Overview about Active Oscillation Damping of Mobile Machine Structure. *Int. J. Fluid Power* **2004**, *5*, 5–24. [[CrossRef](#)]
12. Gianoglio, R.; Salvatore, F.; Weber, J. Method and Device for Damping the Displacement of Construction Machines. U.S. Patent 7756622, 13 July 2010.
13. Alexander, A.; Vacca, A.; Cristofori, D. Active Vibration Damping in Hydraulic Construction Machinery. *Procedia Eng.* **2017**, *176*, 514–528. [[CrossRef](#)]
14. Bell, R.; Pennington, A.D. Active Compensation of Lightly Damped Electrohydraulic Cylinder Drives Using Derivative Signals. *Proc. Inst. Mech. Eng.* **1969**, *84*, 83–98. [[CrossRef](#)]
15. Tongue, B.H. *Principles of Vibration*; Oxford University Press: Oxford, UK, 2002.
16. Guangrong, C.; Junzheng, W.; Shoukun, W.; Jiangbo, Z.; Wei, S. The Separate Meter in Separate Meter Out Control System Using Dual Servo Valves Based on Indirect Adaptive Robust Dynamic Surface Control. *J. Syst. Sci. Complex.* **2019**, *32*, 557–576.
17. Li, C.; Chen, Z.; Yao, B. Identification and adaptive robust precision motion control of systems with nonlinear friction. *Nonlinear Dyn.* **2019**, *95*, 995–1007. [[CrossRef](#)]
18. Wu, X.; Jin, P.; Zou, T.; Qi, Z.; Xiao, H.; Lou, P. Backstepping Trajectory Tracking Based on Fuzzy Sliding Mode Control for Differential Mobile Robots. *J. Intell. Robot. Syst.* **2019**, 1–13. [[CrossRef](#)]
19. Cao, Y.; Huang, J.; Wu, D.; Zhang, M.; Xiong, C. Integration of Nonlinear Disturbance Observer within Proxy-based Sliding Mode Control for Pneumatic Muscle Actuators. *Appl. Sci.* **2019**, *9*, 1571.
20. Wang, C.; Quan, L.; Zhang, S.; Meng, H.; Lan, Y. Reduced-order model based active disturbance rejection control of hydraulic servo system with singular value perturbation theory. *ISA Trans.* **2017**, *67*, 455–465. [[CrossRef](#)] [[PubMed](#)]
21. Choux, M.; Karimi, H.; Hovland, G.; Hansen, M. Robust adaptive backstepping control design for a Nonlinear Hydraulic-Mechanical System. In Proceedings of the 48th IEEE Conference on Decision and Control (CDC), Shanghai, China, 15–18 December 2009; pp. 2460–2467.
22. Hast, M.; Åström, K.J.; Bernhardsson, B.; Boyd, S. PID design by convex-concave optimization. In Proceedings of the 2013 European Control Conference (ECC), Zurich, Switzerland, 17–19 July 2013; pp. 4460–4465.
23. Mercader, P.; Åström, K.J.; Banos, A.; Häggglund, T. Robust PID design based on QFT and convex-concave optimization. *IEEE Trans. Control. Syst. Technol.* **2016**, *25*, 441–452. [[CrossRef](#)]
24. Karimi, A.; Kammer, C. A data-driven approach to robust control of multivariable systems by convex optimization. *Automatica* **2017**, *85*, 227–233. [[CrossRef](#)]
25. Niksefat, N.; Sepehri, N. Design and experimental evaluation of a robust force controller for an electro-hydraulic actuator via quantitative feedback theory. *Control Eng. Pract.* **2000**, *8*, 1335–1345. [[CrossRef](#)]
26. Truong, D.Q.; Ahn, K.K. Force control for hydraulic load simulator using self-tuning grey predictor—Fuzzy PID. *Mechatronics* **2009**, *19*, 233–246. [[CrossRef](#)]
27. Na, J.; Li, Y.; Huang, Y.; Gao, G.; Chen, Q. Output feedback control of uncertain hydraulic servo systems. *IEEE Trans. Ind. Electron.* **2019**, *67*, 490–500. [[CrossRef](#)]
28. Wang, Y.; Wu, H. Adaptive robust backstepping control for a class of uncertain dynamical systems using neural networks. *Nonlinear Dyn.* **2015**, *81*, 1597–1610. [[CrossRef](#)]
29. Jing, C.; Xu, H.; Jiang, J. Dynamic surface disturbance rejection control for electro-hydraulic load simulator. *Mech. Syst. Signal. Process.* **2019**, *134*, 106293. [[CrossRef](#)]
30. Yang, S.; Yin, Q.; Yang, L. Co-simulation of Dynamic Surface Sliding Mode Control for Elevation Equilibrator Electro-Hydraulic System of Truck-Mounted Howitzer. In Proceedings of the 2019 4th International Conference on Automation, Control and Robotics Engineering, Shenzhen, China, 19–21 July 2019; p. 44.

31. Guo, Q.; Shi, G.; Wang, D. Adaptive Composite Fuzzy Dynamic Surface Control for Electro-Hydraulic-System, with Variable-Supply-Pressure. *Asian J. Control* **2019**. [[CrossRef](#)]
32. Wen-Hua, C.; Ballance, D.J.; Gawthrop, P.J.; Reilly, J.O. A nonlinear disturbance observer for robotic manipulators. *IEEE Trans. Ind. Electron.* **2000**, *47*, 932–938. [[CrossRef](#)]
33. Han, J. *Active Disturbance Rejection Control. Technique-The Technique for Estimating and Compensating the Uncertainties*; National Defense Industry Press: Beijing, China, 2008.
34. Shen, W.; Wang, J.; Huang, H.; He, J. Fuzzy sliding mode control with state estimation for velocity control system of hydraulic cylinder using a new hydraulic transformer. *Eur. J. Control.* **2019**, *48*, 104–114. [[CrossRef](#)]
35. Xingxu, W.; Guang, H.; Rui, G. PID Sliding Mode Control for Electro-hydraulic Servo System. *J. Phys. Conf. Ser.* **2019**, *1168*, 022085. [[CrossRef](#)]
36. Kim, J.; Jin, M.; Choi, W.; Lee, J. Discrete time delay control for hydraulic excavator motion control with terminal sliding mode control. *Mechatronics* **2019**, *60*, 15–25. [[CrossRef](#)]



© 2019 by the authors. Licensee MDPI, Basel, Switzerland. This article is an open access article distributed under the terms and conditions of the Creative Commons Attribution (CC BY) license (<http://creativecommons.org/licenses/by/4.0/>).